PERGAMON

Control Engineering Practice 6 (1998) 1193–1208

Automatic current control of magnet cranes for steel plate yard automation

Sang Y. Park[a], Jin S. Lee[a,*], Joon. Y. Choi[a], B. H. Park[b]

[a]*Department of Electrical Engineering, Pohang University of Science and Technology, Pohang 790-784, South Korea*
[b]*Instrumentation & Control Research Team, Technical Research Lab. of Pohang Iron & Steel Co., Pohang, 790-785, South Korea*

Received 29 July 1997

Abstract

This paper presents an automatic current-control method for magnet cranes for thick steel plate yard automation. In moving the steel plates from stack to stack or from stack to shipping truck, it is difficult to lift the correct number of steel plates because the dimensions of the stacked steel plates are in general different, and their other parameters are not completely known and may even vary in a nonlinear fashion. In this paper, recursive form flux equations are first derived for the thick steel plates, and a current equation is then determined for the magnet coil. Based on these equations, an adaptive current predictor is developed to exert the right amount of current on the magnet, so as to lift the correct number of steel plates. When the initial trial with this current fails, a current tuning method is introduced to adjust the current and lift the correct number of plates. The developed magnet current controller has been successfully tested on data obtained from the storage yard at the Pohang Iron & Steel Co. (POSCO).

Keywords: Current control; adaptive current prediction; current tuning; gradient descent algorithm; adaptive fuzzy logic

1. Introduction

Even these days, most of the operations in storage yards for thick steel plates are still carried out by of crane operators, maintenance personnel, etc. In order to increase the cost-competitiveness of steel products, however, there has been increasing interest in recent years in automating all or part of the storage-yard operations (Ohnishi et al., 1981; Yoon et al., 1991; Fliess et al., 1993; Lee and Park, 1994; Lee and Kang, 1996). The thick steel plates are usually produced from steel slabs by rolling them in steps and cutting them in pieces, and are then moved to the storage yard to be shipped later to the customers. In the storage yard, the steel plates are rearranged every day according to the customer order lists, and stacked in such a way that they are convenient to manage and ship to the customer trucks. Fig. 1 shows an overview of the overhead magnet crane used in POSCO, which is similar in structure to a three-axis gantry-type robot.

*Corresponding author. Tel.: 00 82 562 279 2230; fax: 00 82 562 279 2903; e-mail: spart@tau.postech.ac.kr.

The crane body moves along the side rails and the crab moves along the crane body to move the trolley to the requested place. The trolley moves up and down to raise and lower the magnets, and the current applied to the magnet coil attaches and detaches the magnet to and from the given number of steel plates. How many plates are attached to the magnet depends on the amount of current exerted on the magnetic coil. Different dimensions of steel plates could be stacked together in the same stack, according to the order lists and the order of shipment. Thus, given an order to lift a given number of plates, the operator must exert the appropriate amount of current on the magnetic coil to lift them. When lifting the plates, he usually adjusts the amount of current, based on his experience, until the requested number of plates are attached to the magnet. If he fails with this effort, he releases the attached plates back on to the stack, and tries again with different current values. Once the requested number of plates have been lifted, he increases the amount of current to the allowable maximum to keep the steel plates attached, and moves them to the destination stack or to the shipping truck.

0967-0661/98/$ – see front matter
PII: S0967-0661(98)00084-7

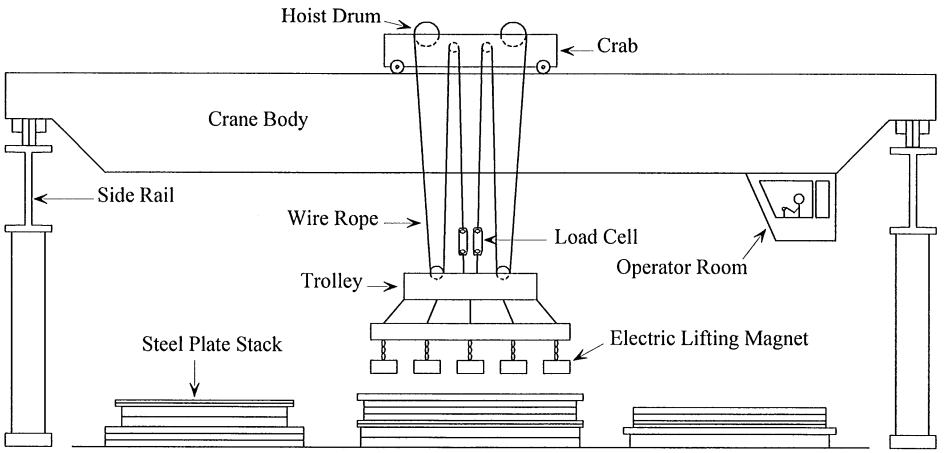

Fig. 1. The overview of overhead magnet crane.

Automating this manual control part of the magnet coil current is known to be one of the most important steps in storage-yard automation. In automating the current-control procedure, at least two components are required: measurement of the number of steel plates being lifted, and prediction of the correct amount of current needed to lift the given number of plates. In determining the number of plates, several measurement devices can be used: load cells (Lee and Park, 1994), sonar sensors, CCD cameras, magnetic flux sensors (Lee and Kang, 1996), etc. Currently, in the steel plate storage yard in POSCO, the load cells are installed as shown in Fig. 1, and used to measure the total weight of the lifted plates and deduce how many plates are lifted. Predicting the correct amount of magnet coil current is important because, once the given number of plates have been lifted with this current, operating time is significantly reduced and the productivity is significantly increased. If the procedure fails, the operator must lower the trolley, detach the steel plates, adjust the current and exert it on the magnetic coil, attach the plates once again, raise the trolley, and check how many plates are attached to the magnet. If this operation is repeated over and over, the time to complete the task is increased, and the productivity is decreased. The amount of predicted current can be computed from a mathematical model formulated by using information about the steel plates, available from the supervisory computer. The relationship between the magnetic force and the magnet coil current is not linear in general, and can be derived by solving rather complex magnetic circuit equations. The recursive form flux equations describing the magnetic circuit for the magnet, as well as for the steel plates, are derived in this paper and then used to develop an appropriate current predictor. However, some parameters and functions describing the magnetic circuit are not known, and could even vary for different steel plates. For example, the magnetization curves of the steel plates and the magnet itself are nonlinear, and are not exactly known. The parameters, such as air-gap distance, cross-sectional area of the flux path, length of the flux path, reluctance of the magnet, etc., are difficult to obtain in advance. These parameters could have different values for different cranes. The derived recursive flux equations with unknown parameters and functions are used to form a current prediction model, and its unknown parameters and functions are updated with the gradient descent rule and an adaptive fuzzy control technique. Fuzzy logic systems are known to be able to approximate any continuous function arbitrarily closely (Wang, 1994, 1997). This development is based on the fuzzy-set theory introduced by Zadeh (1965), and has a built-in mechanism to use the accumulated knowledge of human experts (Takagi and Sugeno, 1985). The adaptive fuzzy logic system used in the current predictor presented in this paper is trained by using the sample data collected off-line from the storage yard and generated on-line during operation. If the predicted current fails to lift the correct number of plates, then a current tuning method has been developed to adjust the amount of current and lift the correct number of plates at the next trial. It would be ideal if it were to succeed at the first trial, but the success rate of even the most experienced operator is less than 80% on the average. The performance of the current predictor developed here outperforms that of the experienced operator, but even the current predictor cannot guarantee a 100% success rate in real operation. Thus, the on-line current tuning algorithm is absolutely necessary as a back-up tool. While adjusting the current, it also generates additional samples as a by-product, to be used later to fine-tune the adaptive current predictor.

The remainder of this paper is organized as follows. In Section 2, a set of recursive form flux equations are derived for the magnet and the steel plates. In Section 3, an adaptive current predictor is developed, based on the gradient descent rule and the adaptive fuzzy logic

technique. In Section 4, a current tuning method is introduced when the first trial fails, and on-line sample generation algorithm is presented. Section 5 shows the simulation results carried out with the data obtained from the storage yard at POSCO. Finally, Section 6 concludes the paper.

2. Recursive form flux equation

2.1. Magnetic force and magnetic circuit equation

In the operation of a magnet crane, the steel plates are lifted by using the magnetic force produced by the current exerted on the magnet coil. The relationship between the magnetic force and the coil current can be derived from the flux that stores the energy in the magnetic field. When the permeability μ_0 of the air (Hayt, 1981) and the flux amount ϕ_g that passes through the air gap are assumed to be constant, then the magnetic force F^m induced between the magnet and the steel plate, or between the steel plates, is given by (Scott, 1966)

$$F^m = \frac{\partial E_{m_g}}{\partial l_g} = \frac{1}{2}\,\phi_g^2 \frac{1}{\mu_0 S_g} \tag{1}$$

where E_{m_g} is the magnetic energy stored in the air gap, l_g is the air gap distance and S_g is the cross-sectional area of the flux path. On the other hand, the magnetomotive force (mmf) generated from the magnet coil current induces flux on the magnet and the steel plates. This relationship is given by $\text{mmf} = NI = R\phi = lH$ (Winch, 1963), where N is the number of turns in the coil winding, I is the current that flows through the coil, R is the reluctance of the magnetic circuit, ϕ is the induced flux, l is the length of the flux path and H is the magnetic field intensity. The magnetic field intensity H here is nonlinearly related to the flux density B, the amount of flux per unit area as shown in Fig. 2 (Scott, 1966). If the magnetization curve is given by $B = f(H)$, then an accurate

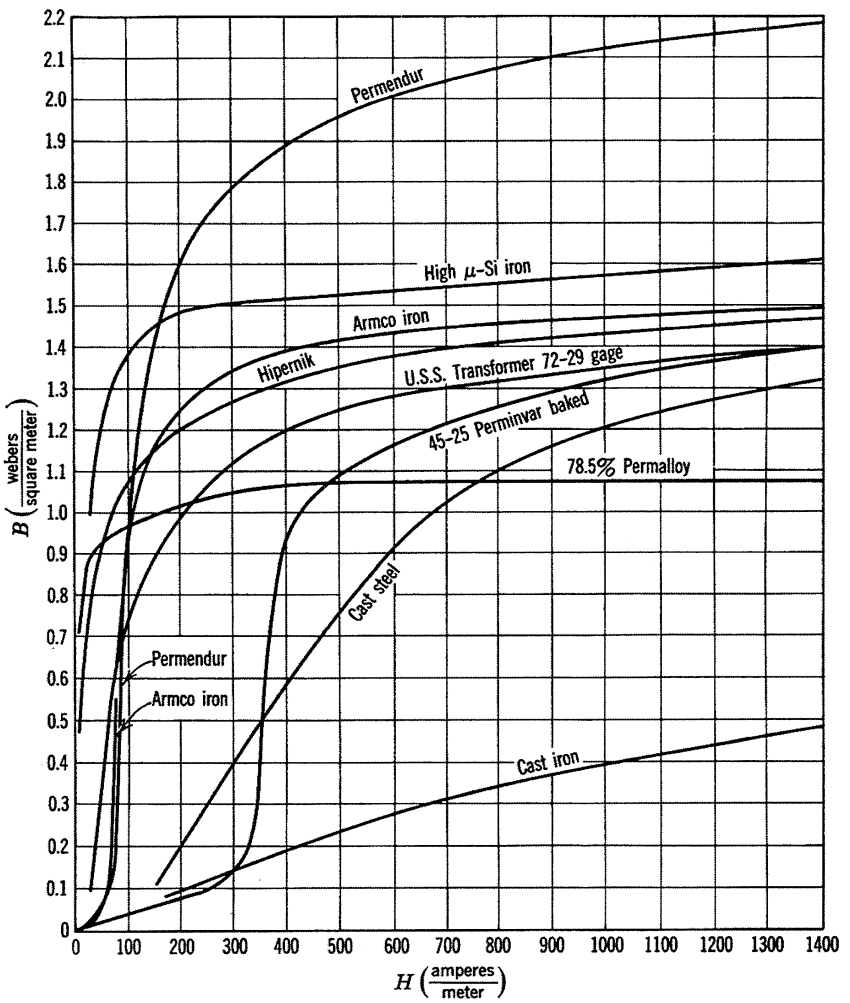

Fig. 2. Magnetization curves for several magnetic materials.

description of the magnetic circuit equation is given by

$$NI = R(\phi)\phi = lf^{-1}(B) = lf^{-1}\left(\frac{\phi}{S}\right), \tag{2}$$

where S is the cross-sectional area of the flux path. f^{-1} in Eq. (2) exists because the magnetization curve is monotonically increasing as shown in Fig. 2.

2.2. Recursive form flux equation

Fig. 3 shows a conceptual drawing of the magnet, with the attached steel plates and the flux path that passes through them. The magnet is one of the five magnets attached to the trolley in Fig. 1, and is used to lift up to 30 tons of steel plates. The steel plates are different in length, width and thickness, and some plates are even narrower than the width of the magnet. In Fig. 3, W_M is the width of the magnet, and l_s is the length of the flux path in the steel plates. p_i for $1 \le i \le n$ denotes the ith steel plate, and W_i, t_i and L_i are, respectively, the width, the thickness and the length of p_i. g_1 is the air gap between p_1 and the magnet, and g_i for $2 \le i \le n$ is the air gap between p_i and p_{i-1}. ϕ_0 is the flux in the magnet, and ϕ_i for $1 \le i \le n$ is the flux in p_i. Fig. 4 shows the magnetic circuit equivalent to Fig. 3. ϕ_{g_i} here is the flux in the air gap g_i, and R_m, R_{p_i} and R_{g_i} are, respectively, the reluctances of the magnet, of the steel plate p_i and of the air gap g_i. R_{g_i} is the sum of the air gap reluctance on the left- and right-hand sides of the flux path in Fig. 3. $R_{p_{i,i+1}}$ denotes the reluctance caused by p_i because ϕ_{g_i+1} traverses down the plate p_i too.

For subsequent development, several assumptions are made about the plant.

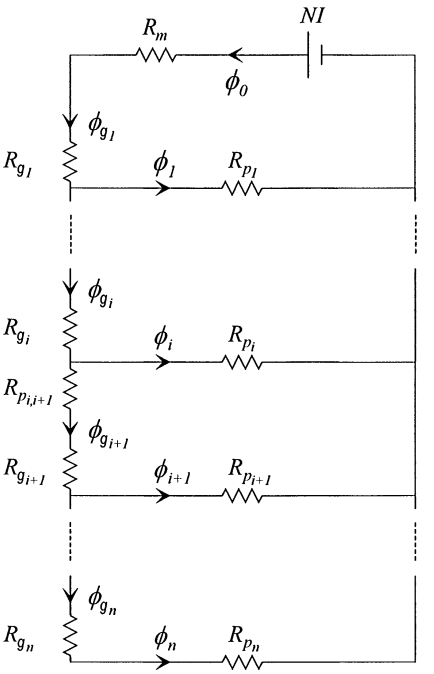

Fig. 4. Equivalent magnetic circuit of Fig. 3.

Assumption 1. *Air gaps $g_1, g_2, \ldots, g_n$ are of the same distance.* The air gaps may differ due to the effect of bending of the steel plates, dust and stains between steel plates, etc., but the differences are usually negligible.

Assumption 2. *Flux permeates the steel plates straight down.* As the magnetic flux permeates deeper through the steel plates, the cross-sectional area of the flux path tends to get larger. But this effect is usually negligible, and the flux is assumed to permeate straight down through the

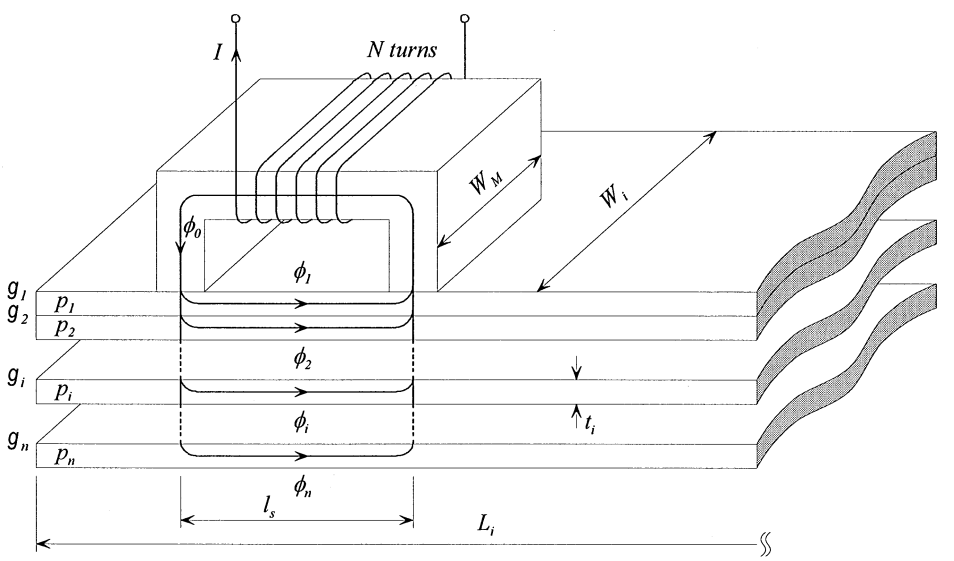

Fig. 3. Flux path of the magnet and steel plates.

steel plates. Thus, in conjunction with Assumption 1, all $R_{g_1}, R_{g_2}, \ldots, R_{g_n}$ are the same as long as the widths of the steel plates $W_1, W_2, \ldots, W_n$ are wider than the magnet width W_M.

Assumption 3. *The leakage flux in the air gap g_{n+1} is negligible.* When n plates are about to be lifted, there remains some attractive force between p_n and p_{n+1}, caused by the leakage flux in the air gap g_{n+1}. This effect may adversely affect p_n, and prevent it from being lifted. Its effect can be taken into account in deriving the required magnet coil current, but is ignored here, to keep the equations simple.

Based on these assumptions, the magnetic flux equations can be derived for each loop in Fig. 4, and hence the resulting equations relate the magnet current I to the parameters of the lifted steel plates in recursive form. First, to lift p_n, the magnetic force induced between p_{n-1} and p_n must be larger than the weight M_n of p_n. Since the magnetic force is generated at both ends of the magnet shoe, it follows from Eq. (1) that

$$F^m_{g_n} = 2\frac{\phi^2_{g_n}}{2\mu_0 S_{g_n}} \geq M_n = g\rho t_n W_n L_n \tag{3}$$

and since $\phi_n = \phi_{g_n}$ in Fig. 4, it follows that

$$\phi_n \geq \sqrt{\mu_0 S_{g_n} g\rho t_n W_n L_n} = \sqrt{\mu_0 \frac{S_0}{W_M} g\rho} \cdot \sqrt{W_{\phi_n} t_n W_n L_n} \tag{4}$$

where g is the gravitational acceleration and ρ is the density of the steel plates. $S_{g_n} = (W_{\phi_n} S_0)/(W_M)$ here is the effective cross-sectional area of the flux path in the air gap g_n, where $W_{\phi_n} = \min[W_M, W_1, W_2, \ldots, W_n]$ is the effective width of the flux path in the air gap g_n and S_0 is the cross-sectional area of the flux path at the bottom of the magnet shoe. W_{ϕ_n} is introduced here since steel plates are sometimes narrower than the magnet, and the width of the flux path then becomes smaller than W_M. S_0 is not known in general because the magnetic core in the magnet is covered with the outer magnet steel slab. By using Eq. (2) repeatedly for each closed loop in Fig. 2, the following equations are generated:

$$NI = R_{p_1}\phi_1 + R_m\phi_{g_1} + R_{g_1}\phi_{g_1} \tag{5}$$

$$R_{p_i}\phi_i = R_{p_{i+1}}\phi_{i+1} + R_{g_{i+1}}\phi_{g_{i+1}} + R_{p_i,i+1}\phi_{g_{i+1}}, \qquad 1 \leq i \leq n-1, \tag{6}$$

where $R_{g_i} = (W_M R_0)/(W_{\phi_i}) = (W_M)/(W_{\phi_i}) \cdot (2l_g)/(\mu_0 S_0)$ and

$$\phi_{g_i} = \phi_i + \phi_{g_{i+1}} = \sum_{k=i}^{n} \phi_k, \qquad 1 \leq i \leq n. \tag{7}$$

R_0 here denotes the reluctance of the air gap g_1 when $W_1 > W_M$. If the magnetization curves of the steel plate and the magnet are given by $B = f_s(H)$ and $B = f_m(H)$, respectively, then Eqs. (5) and (6) can be transformed to the following two equations, Eqs. (8) and (9), as derived in Appendix A:

$$I = \frac{l_s}{N} f_s^{-1}\left(\frac{\phi_1}{t_1 W_{\phi_1}}\right) + \frac{l_m}{N} f_m^{-1}\left(\frac{\phi_{g_1}}{S_m}\right) + \frac{W_M R_0}{N}\frac{\phi_{g_1}}{W_{\phi_1}}, \tag{8}$$

$$\phi_i = \frac{t_i W_{\phi_i}}{t_{i+1} W_{\phi_{i+1}}}\phi_{i+1} + t_i W_{\phi_i} f_s\left(\frac{W_M R_0}{l_s}\frac{\phi_{g_{i+1}}}{W_{\phi_{i+1}}}\right) + \frac{W_M}{l_s S_0} t_i^2 \phi_{g_{i+1}}, \qquad 1 \leq i \leq n-1, \tag{9}$$

where l_m and S_m are, respectively, the length and the cross-sectional area of the flux path in the magnet, and $S_{p_i} = t_i W_{\phi_i}$ for $1 \leq i \leq n$ denotes the effective cross-sectional area of the flux path in the steel plate p_i on the side.

Remark 1 (*Controllability condition of the system*). Note that the developed Eqs. (4), (8) and (9) assume that if ϕ_n is sufficient to lift the last plate p_n, then ϕ_{g_i} for $1 \leq i \leq n-1$ is also sufficient to lift the following $(n-i+1)$ plates. In fact, even if the amount of flux ϕ_{g_n} is sufficient to lift p_n, the flux ϕ_{g_i}, $1 \leq i \leq n-1$ may not be sufficient to lift all the plates p_i through p_n. Particularly when t_i, $1 \leq i \leq n-1$ is very small, the flux can easily penetrate p_i and generate enough ϕ_{g_n} to lift p_n. So, if some of the p_i's are very heavy but thin, and p_n is very light, then it may be possible that ϕ_n is enough to lift p_n but the magnet fails to lift all of the n plates. Increasing the current to overcome this problem may cause more than n plates to be lifted. Therefore, the plates must be stacked in such a way as to prevent this situation from happening. This particular situation can be detected by checking if each ϕ_{g_i} is sufficient after computing all the ϕ_{g_i}'s.

3. Adaptive fuzzy current prediction

Three equations, Eqs. (4), (8) and (9), as derived in the previous section, completely describe the magnetic circuit of Fig. 4. Some of the parameters of these equations, such as t_i, W_i, L_i for $1 \leq i \leq n$ and W_M, are available from the supervisory control computer. But other parameters such R_0, S_0, N, l_s, l_m and the functions f_s, f_m are not completely known, and require to be identified. First note that Eqs. (4), (8) and (9) are equivalent to

$$I = F_1\left(\frac{\phi_1}{t_1 W_{\phi_1}}\right) + F_2(\phi_{g_1}) + a\frac{\phi_{g_1}}{W_{\phi_1}}, \tag{10}$$

$$\phi_i = \frac{t_i W_{\phi_i}}{t_{i+1} W_{\phi_{i+1}}}\phi_{i+1} + t_i W_{\phi_i} F_3\left(\frac{\phi_{g_{i+1}}}{W_{\phi_{i+1}}}\right) + b t_i^2 \phi_{g_{i+1}}, \quad 1 \leq i \leq n-1 \tag{11}$$

$$\phi_n \geq c\sqrt{W_{\phi_n} t_n W_n L_n}, \tag{12}$$

where $a = W_M R_0/N$, $b = W_M/(l_s S_0)$, $c = \sqrt{\mu_0(S_0/W_M)g\rho}$ are unknown constant parameters and $F_1(\cdot) = (l_s/N) f_s^{-1}(\cdot)$, $F_2(\cdot) = (l_m/N) f_m^{-1}(1/S_m \cdot)$, $F_3(\cdot) = f_s(W_M R_0/l_s \cdot)$ are unknown single-input, single-output (SISO) functions. Now a good current prediction model can be developed for system of Eqs. (10)–(12) once the unknown parameters a, b, c and the unknown functions F_1, F_2, F_3 are replaced with their appropriate estimates. Thus, an appropriate current-prediction model that estimates the minimum required current I_n to lift n plates is of the form:

$$I_n = \hat{F}_1\left(\frac{\phi_1}{t_1 W_{\phi_1}}\right) + \hat{F}_2(\phi_{g_1}) + \hat{a}\frac{\phi_{g_1}}{W_{\phi_1}} \tag{13}$$

$$\phi_i = \frac{t_i W_{\phi_i}}{t_{i+1} W_{\phi_{i+1}}}\phi_{i+1} + t_i W_{\phi_i}\hat{F}_3\left(\frac{\phi_{g_{i+1}}}{W_{\phi_{i+1}}}\right) + \hat{b} t_i^2 \phi_{g_{i+1}}, \quad 1 \le i \le n-1 \tag{14}$$

$$\phi_n = \hat{c}\sqrt{W_{\phi_n} t_n W_n L_n} \tag{15}$$

where $\hat{F}_1$, $\hat{F}_2$ and $\hat{F}_3$ are, respectively, the estimated functions of F_1, F_2 and F_3, and $\hat{a}$, $\hat{b}$ and $\hat{c}$ are, respectively, the estimated parameters of a, b and c. The current I_n resulting from the prediction model of Eqs. (13)–(15) is the minimum current needed to lift n plates because the inequality in Eq. (12) is replaced with the equality in Eq. (15). Note here that the model of Eqs. (13)–(15) fully exploits the particular structure of the original magnetic circuit Eqs. (10)–(12), and the problem of identifying the current-prediction system is reduced to that of estimating the parameters a, b, c and the SISO functions F_1, F_2, F_3. The computed minimum current I_n is not directly applied to the magnet to lift the steel plates, but is used to determine the actual current command I_a as described in the next section. The structure of the developed minimum current predictor is shown in Fig. 5. The prediction unit 1 simply estimates $\hat{c}$, the prediction unit 2 estimates $\hat{b}$ and $\hat{F}_3$, and the prediction unit 3 estimates $\hat{a}$, $\hat{F}_1$ and $\hat{F}_2$. Note here that the prediction unit 2 is used repeatedly for $(n-1)$ stages to compute ϕ_i for $1 \le i \le n-1$.

The unknown parameters a, b and c are estimated in this paper by using the gradient descent algorithm, in which the estimates $\hat{a}$, $\hat{b}$ and $\hat{c}$ are updated in the direction toward minimizing the cost criterion

$$E = \tfrac{1}{2}(I_n^d - I_n)^2, \tag{16}$$

where I_n^d denotes the desired minimum current measured from the real crane. More precisely, $\hat{a}$ in Eq. (13), $\hat{b}$ in Eq. (14) and $\hat{c}$ in Eq. (15) are updated, respectively, as

$$\hat{a}(k+1) = \hat{a}(k) - \eta\frac{\partial E}{\partial \hat{a}} = \hat{a}(k) - \eta\frac{\partial E}{\partial I_n}\frac{\partial I_n}{\partial \hat{a}} = \hat{a}(k) + \eta(I_n^d - I_n)\frac{\phi_{g_1}}{W_{\phi_1}} \tag{17}$$

$$\hat{b}(k+1) = \hat{b}(k) - \eta\frac{\partial E}{\partial \hat{b}} = \hat{b}(k) - \eta\sum_{i=1}^{n-1}\frac{\partial E}{\partial I_n}\frac{\partial I_n}{\partial \phi_i}\frac{\partial \phi_i}{\partial \hat{b}} = \hat{b}(k) + \eta(I_n^d - I_n)\sum_{i=1}^{n-1}\frac{\partial I_n}{\partial \phi_i} t_i^2 \phi_{g_{i+1}}, \tag{18}$$

$$\hat{c}(k+1) = \hat{c}(k) - \eta\frac{\partial E}{\partial \hat{c}} = \hat{c}(k) - \eta\frac{\partial E}{\partial I_n}\frac{\partial I_n}{\partial \phi_n}\frac{\partial \phi_n}{\partial \hat{c}} = \hat{c}(k) + \eta(I_n^d - I_n)\frac{\partial I_n}{\partial \phi_n}\sqrt{W_{\phi_n} t_n W_n L_n}, \tag{19}$$

where $\eta > 0$ is an adaptation gain and the term $\partial I_n/\partial \phi_i$ for $1 \le i \le n$ is derived in Appendix B. On the other hand, the unknown functions F_1, F_2 and F_3 are approximated in this paper by using fuzzy logic systems constructed with Gaussian membership functions, a product inference engine, a singleton fuzzifier, and a center average defuzzifier as described in Wang (1994, 1997). When

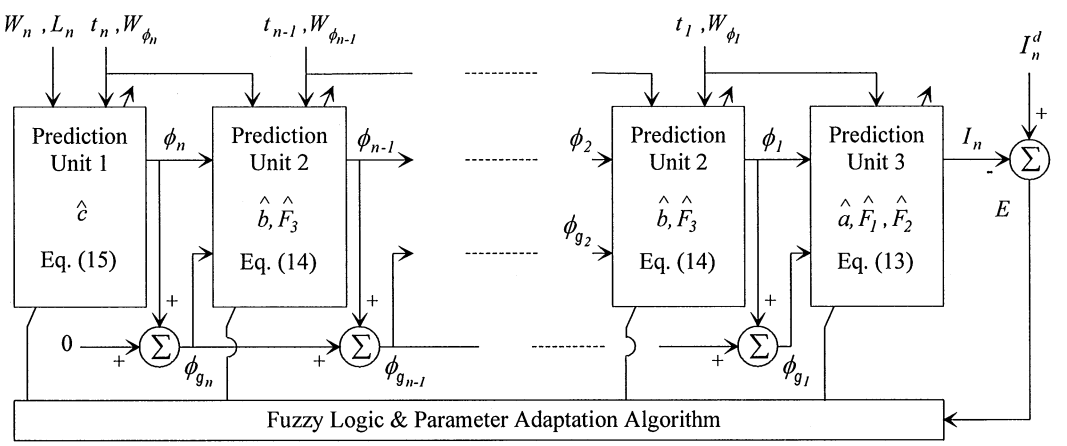

Fig. 5. The structure of adaptive fuzzy minimum current predictor.

these components are combined together, the resulting fuzzy-logic system for given input x is of the form:

$$\hat{F}(x) = \frac{\sum_{r=1}^{M} \bar{y}^r \exp\left(-\left(\frac{x - \bar{x}^r}{\sigma^r} \right)^2 \right)}{\sum_{r=1}^{M} \exp\left(-\left(\frac{x - \bar{x}^r}{\sigma^r} \right)^2 \right)} \tag{20}$$

where M is the number of fuzzy rules, $\bar{y}^r$ is the representative output value for the rth rule, and $\bar{x}^r$ and σ^r are, respectively, the center and the standard deviation of the Gaussian membership function for the premise part of the rth rule. This particular type of fuzzy-logic system is computationally simple and intuitively plausible. Moreover, it is differentiable, and the gradient descent algorithm can be used to update its parameters. The parameters of the fuzzy-logic systems $\hat{F}_1$, $\hat{F}_2$ and $\hat{F}_3$ are also updated in the direction toward minimizing the cost criterion Eq. (16). As shown in Eq. (20), the fuzzy-logic systems $\hat{F}_1, \hat{F}_2$ and $\hat{F}_3$ are completely identified by three sets of parameters: $\bar{x}_m^1, \ldots, \bar{x}_m^M, \sigma_m^1, \ldots, \sigma_m^M$, and $\bar{y}_m^1, \ldots, \bar{y}_m^M$ for $1 \le m \le 3$. In order to simplify its updating procedure, however, its premise part is assumed to be fixed, and only the conclusion part is updated. This is equivalent to saying that all of $\bar{x}_m^1, \ldots, \bar{x}_m^M$ and $\sigma_m^1, \ldots, \sigma_m^M$ are fixed, and only $\bar{y}_m^1, \ldots, \bar{y}_m^M$ are updated. This technique is widely known as the "fuzzy basis function approach", and is described in more detail in Wang (1994, 1997). The updating rule of $\bar{y}_m^r$ for every $1 \le m \le 3$ and $1 \le r \le M$ is equivalent to those of $\hat{a}$, $\hat{b}$ and $\hat{c}$ and is given by

$$\begin{aligned} \bar{y}_m^r(k+1) &= \bar{y}_m^r(k) - \eta \frac{\partial E}{\partial \bar{y}_m^r} = \bar{y}_m^r(k) - \eta \frac{\partial E}{\partial \hat{F}_m} \frac{\partial \hat{F}_m}{\partial \bar{y}_m^r} \\ &= \bar{y}_m^r(k) - \eta \frac{\partial E}{\partial \hat{F}_m} \frac{z_m^r}{\sum_{r=1}^{M} z_m^r}, \end{aligned} \tag{21}$$

where $z_m^r = \exp(-((x - \bar{x}_m^r)/\sigma_m^r)^2)$, and $\partial E/\partial \hat{F}_1$, $\partial E/\partial \hat{F}_2$ and $\partial E/\partial \hat{F}_3$ in Eq. (21) are derived in Appendix C.

4. Current tuning and on-line generation of training samples

The training of the adaptive fuzzy current predictor consists of two stages. One is the off-line training with the sampled data obtained from POSCO's steel-plate storage yard, and the other is on-line training with the off-line data plus newly generated sample data obtained during on-line operation. The off-line data is collected by using the real magnet cranes from different representative steel plate stacks. When collecting the sample data, the operator tries several different current values in order to determine the minimum current value to lift the requested number of plates in the stacks. The measured value of the minimum current is recorded, along with the number and information on the plates, and used as a sample for training the fuzzy current predictor. When a number of sample data are collected from the storage yard, the parameters of the fuzzy current predictor are trained in such a way that the cost criterion

$$E^p = \tfrac{1}{2}(I_n^{dp} - I_n^p)^2 \tag{22}$$

is minimized for each $p = 1, 2, \ldots, \mathscr{P}$, where $\mathscr{P}$ is the total number of collected samples. Once the training has been completed, the current predictor (13)–(15) computes the minimum current I_n and I_{n+1} to lift n and $(n+1)$ steel plates, respectively, from the given stack, from which the current I_a to be applied to the magnet is computed as

$$I_a = \tfrac{1}{2}(I_n + I_{n+1}). \tag{23}$$

Computing I_a in this way and applying it to the magnet, the operator should be able to achieve maximum robustness to various system uncertainties, and in all probability, lift the requested number of plates. In reality, however, there could be many factors that hinder correct prediction of the current. First of all, it is difficult to obtain comprehensive data that cover all dimensions of the steel plates. Moreover, different cranes have different values on their parameters, and even the same shape of steel plates vary in their parameter values. Thus, it is quite possible that the predicted current will fail, and it must be adjusted and tried again. In adjusting the current, a simple but fast algorithm is usually required to complete the task in time. If it fails again, then the adjustment process continues until it succeeds. Each time it fails, a new training sample is generated and stored in the controller, to be used later for on-line training of the current predictor. Once the correct number of plates have been lifted, the accumulated new samples are used together with the original samples to update the current predictor. The updating procedure can be carried out on-line while the crane moves to another steel plate stack for a new task, or it can be done off-line, with the copied version of the current predictor and its updated parameters being copied back to the acting current predictor.

The current tuning and on-line sample-generation algorithm is explained here with the two examples as shown in Fig. 6, and is formalized in Figs. 7 and 8 in the form of pseudo-codes. I_n^* in Fig. 6 denotes the unknown actual minimum current required to lift n plates, and the gray region represents the actual acceptable current range to lift n plates. Fig. 6 then shows how the current tuner generates $I_a(k)$ to lift the requested number of plates. Now let n^r denote the requested number of plates to lift, n^a the number of plates that the current predictor attempts to lift, and n^l the number of plates actually lifted. Thus, whenever $n^l = n^r$, it succeeds, and the task is completed.

First consider the simple and regular case as in Fig. 6a, and assume that I_n^*'s and I_n's are related as shown in the figure, and n plates are requested to be

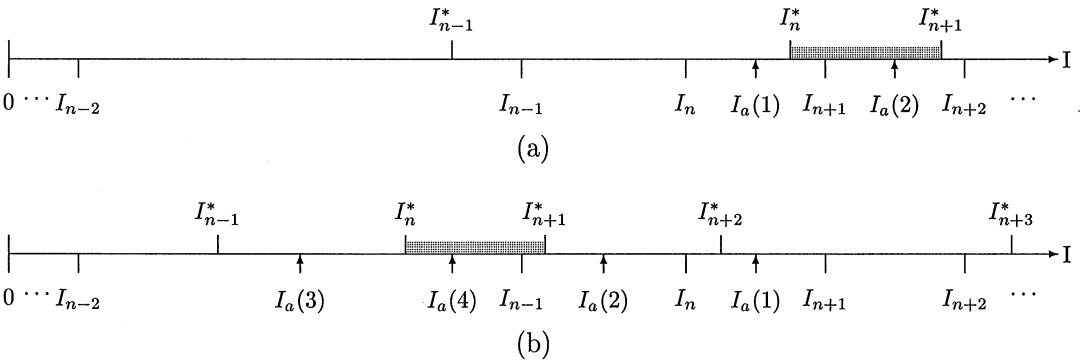

Fig. 6. The presumed relationship of I^*_n's, I_n's and the resulting outcome of $I_a(k)$'s.

$k = 1$; $p = \mathscr{P} + 1$; $n^a(k) = n^r$

LABEL1:

Apply $I_a(k) = \frac{1}{2}(I_{n^a(k)} + I_{n^a(k)+1})$ and determine $n^l(k)$.

/* on-line sample generation part */

If $n^l(k) < n^a(k)$ **then**

Save $I^{dp}_{n^l(k)+1} = I_a(k)$ with the info. of p_i, $1 \le i \le n^l(k) + 1$.

$p = p + 1$

else if $n^l(k) > n^a(k)$ **then**

Save $I^{dp}_{n^l(k)} = I_a(k)$ with the info. of p_i, $1 \le i \le n^l(k)$.

$p = p + 1$

/* current tuning part */

if $n^l(k) = = n^r$ **then**

return SUCCESS

else if $n^l(k) < n^r$ **then**

if† $k > 1$ **and** $n^l(k-1) > n^r$ **then**

goto BISEC_SEARCH in Fig. 8

else

$n^a(k+1) = n^a(k) + 1$

else if $n^l(k) > n^r$ **then**

if† $k > 1$ **and** $n^l(k-1) < n^r$ **then**

goto BISEC_SEARCH in Fig. 8

else

$n^a(k+1) = n^a(k) - 1$

$k = k + 1$
goto LABEL1

Fig. 7. Current tuning and on-line training-sample-generation algorithm.

BISEC_SEARCH:

$lower = \min[I_a(k), I_a(k-1)]$; $upper = \max[I_a(k), I_a(k-1)]$

$k = k + 1$

LABEL2:

Apply $I_a(k) = \frac{1}{2}(lower + upper)$ and determine $n^l(k)$.

if $n^l(k) = = n^r$ **then**

return SUCCESS

else if $n^l(k) < n^r$ **then**

$lower = I_a(k)$;

else if $n^l(k) > n^r$ **then**

$upper = I_a(k)$;

$k = k + 1$
goto LABEL2

Fig. 8. Bisection search part of current tuner.

lifted. Then $n^r = n$ and a natural strategy is to set $n^a = n$ and try $I_a(1) = \frac{1}{2}(I_{n^a} + I_{n^a+1}) = \frac{1}{2}(I_n + I_{n+1})$. Note here that $I_n < I_a(1) < I_{n+1}$. Fig. 6a then shows that $I^*_{n-1} < I_a(1) < I^*_n$, and $(n-1)$ plates are actually lifted. Thus $n^l = n - 1 < n^r$, and it fails. Since $n^l \neq n^a$ and $n^l < n^a$, and $I_n < I_a(1) < I^*_n$ in this case, $I_a(1)$ is closer to I^*_n than I_n is, and is considered as a better candidate to represent the unmeasurable I^*_n. In this case, I^{dp}_n is set to $I_a(1)$, and is saved as a new item of sample data for further training. Here p is set to $(\mathscr{P} + s + 1)$, where s is the number of previously accumulated samples generated during on-line operation. In the original sampled data collected off-line from the storage yard, each minimum current is actually measured by repeated trials, and is saved as I^{dp}_n. During on-line operation, however, the operator does not have enough time to repeat the trials to determine the best possible minimum current, and $I_a(1)$ is simply assumed to represent I^*_n, and is saved as a new I^{dp}_n. Since $I_n < I^{dp}_n = I_a(1) < I^*_n$ and it is used for further training, it will update the fuzzy system in such a way that the newly predicted I_n becomes larger than the current I_n and gets closer to I^*_n. Now that $n^l < n^r$, increase n^a by one and set $n^a = n + 1$, and try

$I_a(2) = \frac{1}{2}(I_{n+1} + I_{n+2})$. As shown in Fig. 6a, $I_a(2)$ is then within the acceptable current range, and it succeeds. Thus $n^l = n = n^r$, and the task is completed. But $n^l < n^a$ even in this case, and since $I_{n+1} < I_a(2) < I^*_{n+1}$, $I^{d(p+1)}_{n+1}$ is set to $I_a(2)$ and is saved as a new sample. If it fails again and $(n-1)$ plates are lifted, then the current tuner overwrites I^{dp}_n with $I_a(2)$ without increasing the index number p. Then set $n^a = n+2$ and $I_a(3) = \frac{1}{2}(I_{n+2} + I_{n+3})$, and continue the search until it succeeds. Note here that the samples are generated on-line whenever $n^l \neq n^a$, while the current tuning continues until the condition $n^l = n^r$ is met.

Next consider the more intriguing case as shown in Fig. 6b, and assume that n plates are requested. Then $n^r = n$ and a natural strategy is to set $n^a = n$ and try $I_a(1) = \frac{1}{2}(I_n + I_{n+1})$. Fig. 6b then shows that $I^*_{n+2} < I_a(1) < I^*_{n+3}$, and $(n+2)$ plates are actually lifted. Thus $n^l = n+2 > n^r$ and it fails. Since $n^l \neq n^a$ and $n^l > n^a$, and $I^*_{n+2} < I_a(1) < I_{n+1} < I_{n+2}$ in this case, $I_a(1)$ is closer to I^*_{n+2} than I_{n+2} is, and is considered as a better candidate to represent the unmeasurable I^*_{n+2}. In this case, I^{dp}_{n+2} is set to $I_a(1)$ and is saved as a new sample data for training. In contrast with the previous example, $I^*_{n+2} < I^{dp}_{n+2} = I_a(1) < I_{n+2}$ and, if it is used for further training, it will update the fuzzy system in such a way that the newly predicted I_{n+2} becomes smaller than the current I_{n+2} and gets closer to I^*_{n+2}. Quite possibly, the newly predicted I_{n+1} and I_n will also get closer to I^*_{n+1} and I^*_n, respectively. Now that $n^l > n^r$, decrease n^a by one, i.e., set $n^a = n-1$ and try $I_a(2) = \frac{1}{2}(I_{n-1} + I_n)$. Even in this case, it fails again with $n^l = n+1 > n^r$. Since $n^l > n^a$ and $I^*_{n+1} < I_a(2) < I_n < I_{n+1}$, $I^{d(p+1)}_{n+1}$ is set to $I_a(2)$ and is saved as a new sample. Now set $n^a = n-2$ and try $I_a(3) = \frac{1}{2}(I_{n-2} + I_{n-1})$. This time, only $(n-1)$ plates are lifted, and it fails again with $n^l = n-1 < n^r$. But, once again, $n^l > n^a$ and, since $I^*_{n-1} < I_a(3) < I_{n-1}$, $I^{d(p+2)}_{n-1}$ is set to $I_a(3)$ and is saved as a new sample. Now the operator must try a current somewhere between $I_a(2)$ and $I_a(3)$ to lift n plates. At this point, the so-called 'bisection method' (Atkinson, 1993) is used to determine $I_a(4) = \frac{1}{2}(I_a(2) + I_a(3))$. When it is applied to the magnet, it finally succeeds, and the task is completed. Once the task has been successfully completed, the on-line training of the adaptive fuzzy current predictor starts with the newly generated plus the original samples, and the parameters of the current predictor are updated accordingly.

The on-line sample-generation algorithm outlined in the previous examples can be formalized in a more general case. First, note that

$$I_{n^a} < I_a(k) < I_{n^a+1} \tag{24}$$

since $I_a(k) = \frac{1}{2}(I_{n^a} + I_{n^a+1})$ and

$$I^*_{n^l} < I_a(k) < I^*_{n^l+1} \tag{25}$$

since n^l plates are lifted. Now, if $n^l < n^a$, then $I_{n^l} < I_{n^l+1} \leq I_{n^a}$ and, from Eqs. (24) and (25), $I_{n^l+1} \leq I_{n^a} < I_a(k) < I^*_{n^l+1}$ follows. Thus $I_a(k)$ is considered as a better candidate for $I^*_{n^l+1}$, and $I^{dp}_{n^l+1}$ is set to $I_a(k)$ and is saved as a new sample. In contrast, if $n^l > n^a$, then $I_{n^a} < I_{n^a+1} \leq I_{n^l}$ and, from Eqs. (24) and (25), it follows that $I^*_{n^l} < I_a(k) < I_{n^a+1} \leq I_{n^l}$. Thus, $I_a(k)$ is considered as a better candidate for $I^*_{n^l}$ and $I^{dp}_{n^l}$ is set to $I_a(k)$, and is saved as a new sample.

Figs. 7 and 8 show the pseudo-codes of the algorithm that describes the current-tuning procedure and on-line generation of training samples. Fig. 7 shows the on-line sample-generation part in the first **if-else if** block, and the current-tuning part in the second **if-else if** block. The **if**† command in the current-tuning part checks if $I_a(k)$ has bypassed the acceptable current range. Fig. 8, on the other hand, shows the bisection search routine used in the current-tuning procedure.

5. Simulation results

In order to show the feasibility of the developed current predictor and tuner, several simulation tests have been performed on a computer using the sample data obtained from the No. 2 storage yard of thick steel plates at POSCO. Since these data have been actually measured and collected from a real crane in the storage yard and not computed from its mathematical model, they reflected various uncertainties such as sensor noises, dust, stains, air-gap variances, fringing field effects of the flux, leakage flux effects and other factors. Thus, the developed fuzzy-current predictor trained with these experimental data tends to reflect the real situation, rather than its mathematical model.

W_M is given *a priori* from the supervisory computer, and is set to 1.9 m for this simulation example. The crane lifts up to 30 t of total weight, and each magnet applies current up to 20 A. Thus, each trolley with five magnets can apply current up to 100 A in total. The magnet cranes lift steel plates only up to 50 mm in total thickness. Sixty data samples have been collected from the storage yard and used for the off-line training of the fuzzy current predictor. The steel plates in the sample data range from 6 to 50 mm in thickness, 1.64–3.05 m in width, 3.5–12 m in length and 525–8472 kg in weight. These sample data were selected and obtained from one week of real operation of one crane in the storage yard. The collected samples indeed cover a wide variety of plate stacks. They even included extreme stacks where they consist of a very thick plate over a very thin one, or *vice versa*. The stacks are extreme cases because, when the order of stacked plates is changed, the currents to be applied to lift them are quite different, even if they are of the same weight. In the present manual operation, these are the tasks which the human operator cannot handle very well.

Ten membership functions are used to describe the fuzzy identifiers $\hat{F}_1$, $\hat{F}_2$ and $\hat{F}_3$. The Gaussian

membership functions of $\hat{F}_1$ are $\exp(-((x-\bar{x}_1^r)/\sigma_1^r)^2)$, $1 \le r \le 10$. $\hat{F}_1$ is initially approximated as a first-order polynomial with the parameters $\bar{y}_1^r = (r-1)\frac{0.5}{9}$, $\bar{x}_1^r = (r-1)\frac{1.5}{9}$ and $\sigma_1^r = 1.3$ for $1 \le r \le 10$. The parameters of $\hat{F}_2$ are initially set to $\bar{y}_2^r = (r-1)\frac{5}{9}$, $\bar{x}_2^r = (r-1)\frac{1}{9}$, $\sigma_2^r = 0.087$ for $1 \le r \le 10$, and the parameters of $\hat{F}_3$ are initially set to $\bar{y}_3^r = (r-1)\frac{0.5}{9}$, $\bar{x}_3^r = (r-1)\frac{0.5}{9}$, $\sigma_3^r = 0.043$ for $1 \le r \le 10$. In the gradient descent algorithm, the adaptation gain η was set to 1×10^{-5} for every estimation.

Figs. 9 and 10 show the simulation results of the fuzzy current predictor trained with only the original samples obtained from the field. The on-line training-sample-generation algorithm is not used in this case. As the iteration continues, the average absolute error reduces to 0.9A, as shown in Fig. 9, and the success rate of the first trial approaches 98%, as shown in Fig. 10. The results verify that the developed flux equations are valid, and that the assumptions made about the system are reasonable. Since the success rate of human experts with more than 10 years of experience is about 75 ~ 80% at the first trial, the performance of the developed adaptive fuzzy current predictor is excellent. An average absolute error of 0.9A is relatively small, compared with the current range of 50A in regular operation. But considering the fact that the difference between the current values to lift one 6 mm-thick plate and two 6 mm-thick plates is only 0.6A, the value of the average absolute error looks rather big in Fig. 9, and keeps the success rate from approaching 100%. Quite possibly, this error is caused by many uncertain factors in the current magnet system and the steel plates.

Figs. 11–14 show the simulation results when the additional samples obtained during on-line operation are used together with the original samples. In the first round of training, the simulation starts with the original 60 samples and, in order to learn the inherent dynamics as far as possible, 30,000 iterations are performed to train the current predictor.

Then the predictor is put to the test with the original samples, and whenever the predictor fails to predict the correct current, a new sample is generated. After the test has been completed, five new samples are generated and the total of 65 samples are available for the next round of training. Another 30,000 iterations of training are then performed with 65 samples, and the resulting adjusted predictor is again tested. This step is carried out over and over. After the third testing period, the total number of training samples increases to 69 as shown in Fig. 13, with a 100% success rate as shown in Fig. 12. Note that the time it takes to reach this success rate is shorter than that it takes to reach a 98% success rate in Fig. 10, where there was no sample-generation mechanism. Fig. 14 shows that even before the success rate reaches 100%, the current tuner completes the task at the second or third trial.

Figs. 15–18 show another interesting simulation result, where the original samples are never used for training. The off-line training of the current predictor is omitted and, from the beginning, the test operation of the current

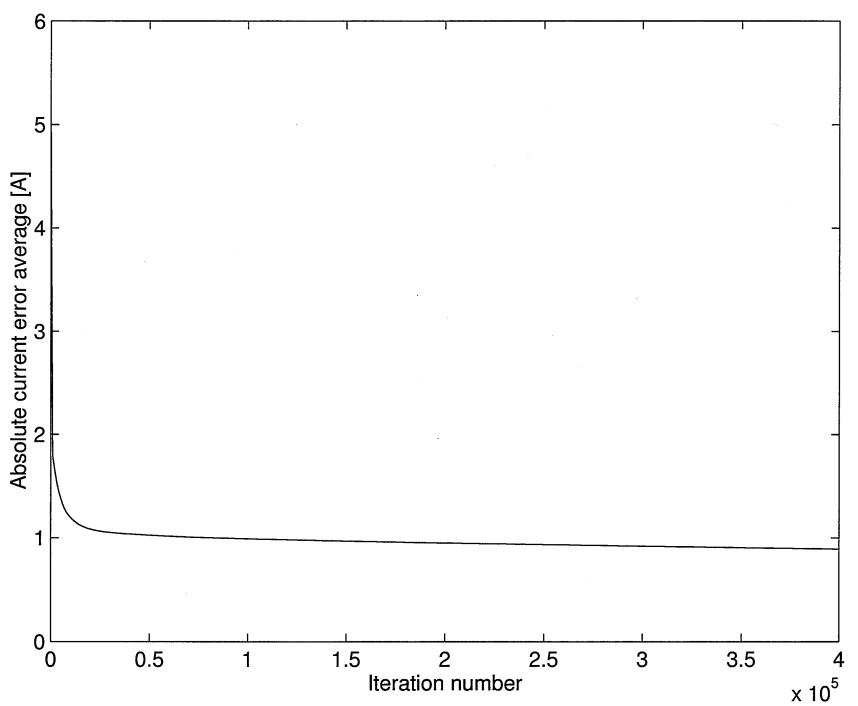

Fig. 9. Absolute current error average of the current predictor trained with only the original samples.

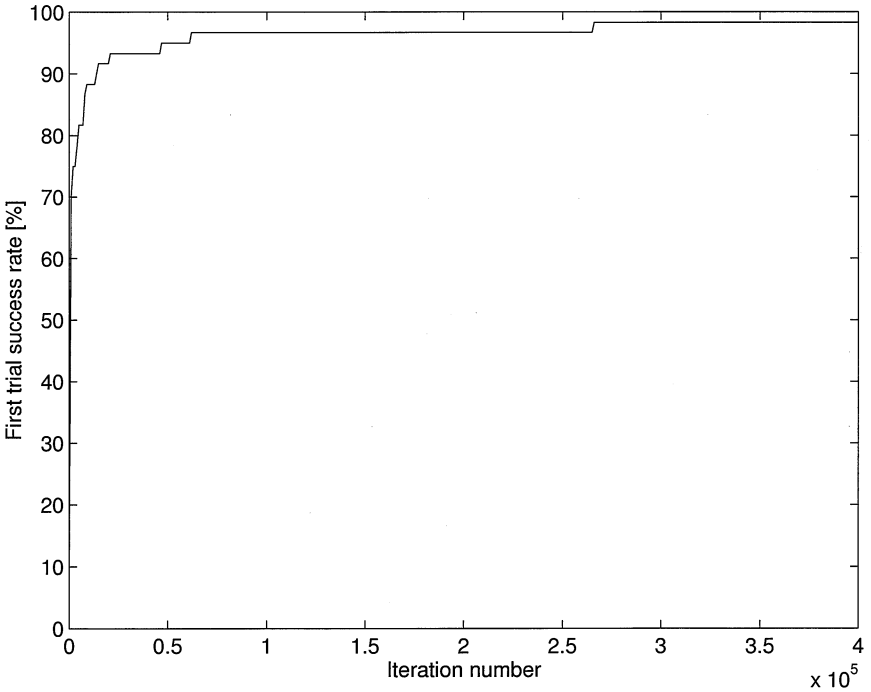

Fig. 10. First trial success rate of the current predictor trained with only the original samples.

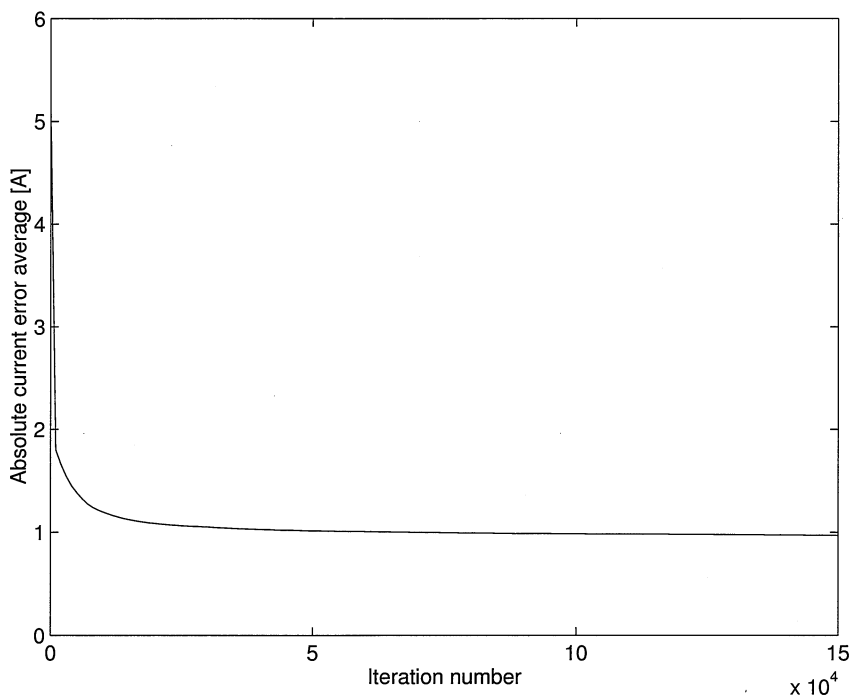

Fig. 11. Absolute current error average of the current predictor trained with the original plus the on-line samples.

predictor is carried out, and a set of new samples are generated and are used for the training of the predictor. In contrast with the previous case where the training is started with the off-line samples, this simulation is carried out without any off-line samples, and hence can be considered as a unsupervised learning mechanism. It is shown in Figs. 15–18 that even in this case the success rate approaches 95%, though it takes longer and the total number of training samples increases to 290. The average absolute error of Fig. 15 is bigger than those of

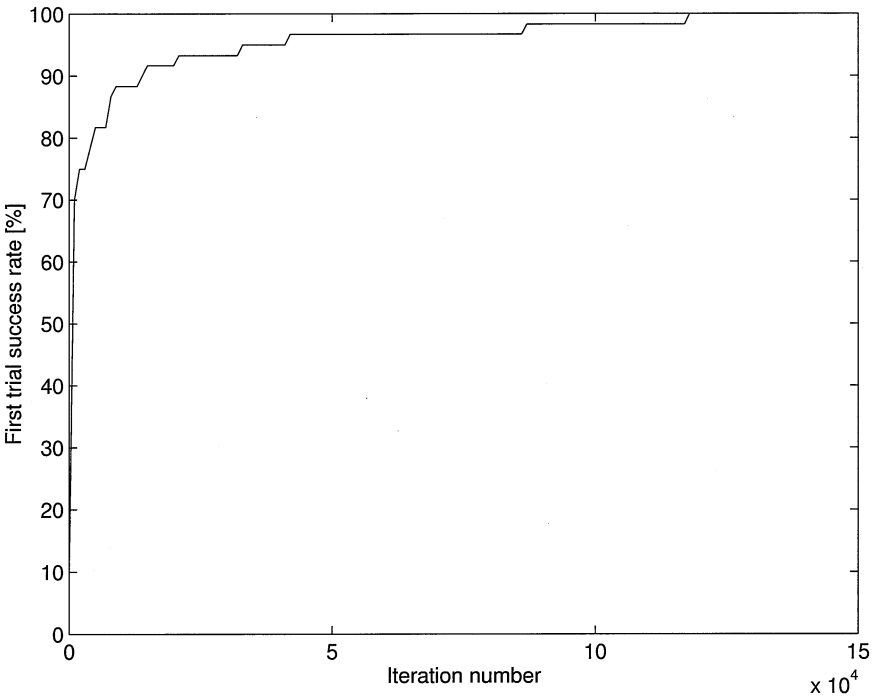

Fig. 12. First trial success rate of the current predictor trained with the original plus the on-line samples.

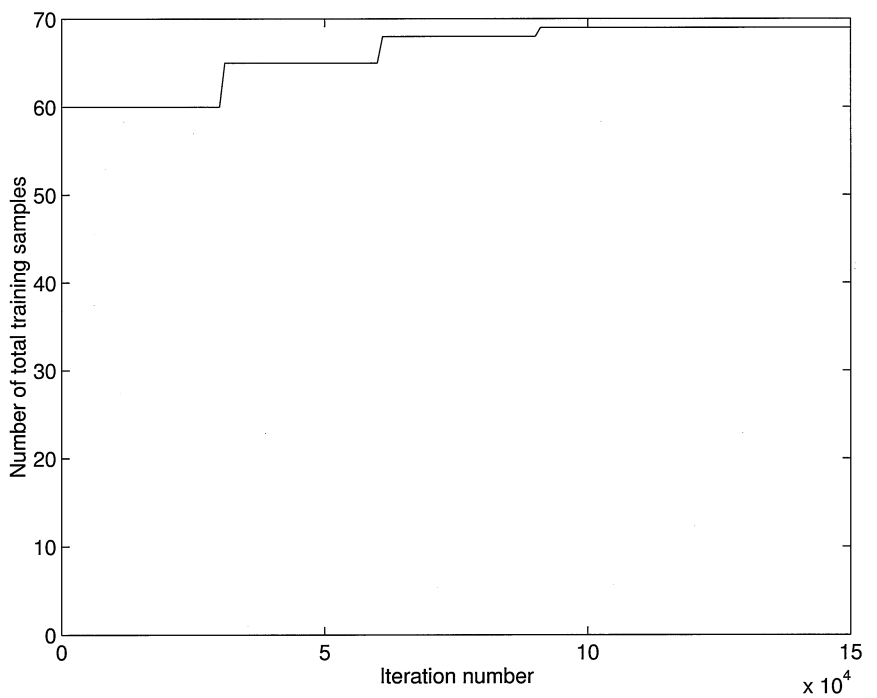

Fig. 13. Total number of original plus on-line samples.

Figs. 9 and 11, but this is not a serious issue because the ultimate goal of the current predictor is to lift the desired number of steel plates within the minimum time. Fig. 18 shows the average number of trials required to complete the task when the first trial fails, which remains within 3 and converges to 2. These results show that the proposed current predictor and tuner can be applied to the real system even without collecting the initial training samples, which requires much time and effort of the field operator.

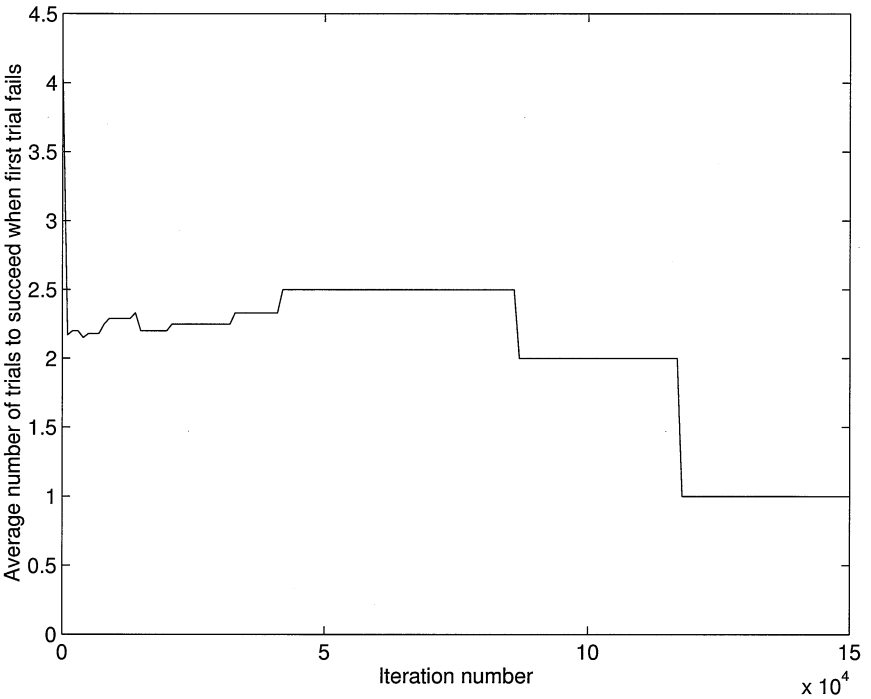

Fig. 14. Average number of trials required to complete the task when the first trial fails. (The current predictor is trained with the original plus the on-line samples.)

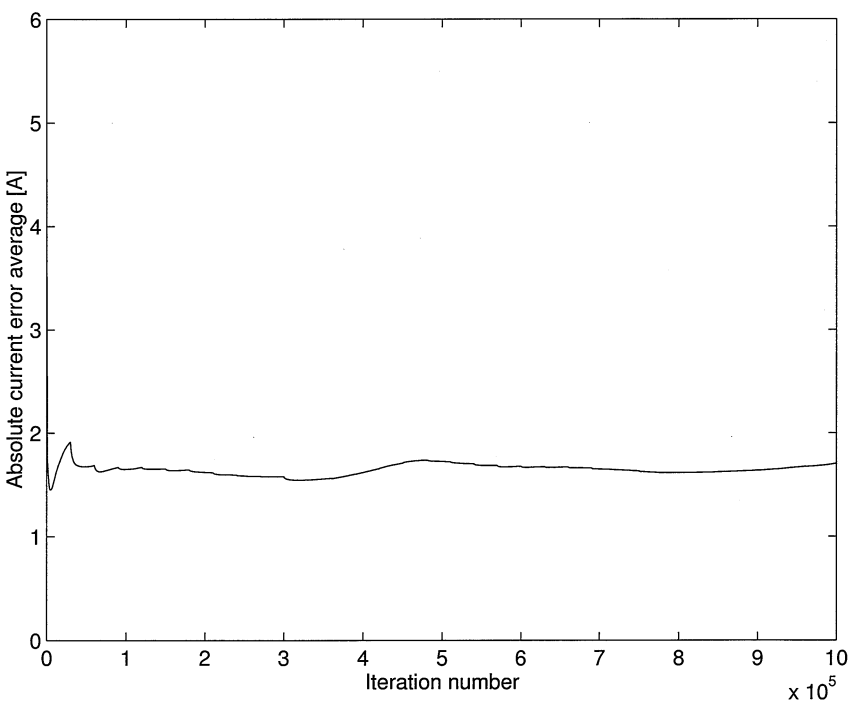

Fig. 15. Absolute current error average of the current predictor trained with only the on-line samples.

6. Conclusion

In this study, an adaptive current predictor and a current tuner have been developed to estimate and adjust the magnet current to lift the correct number of steel plates, and then to automate the steel-plate storage and shipping procedure. Recursive form flux equations are derived first, and used as the base equations to construct

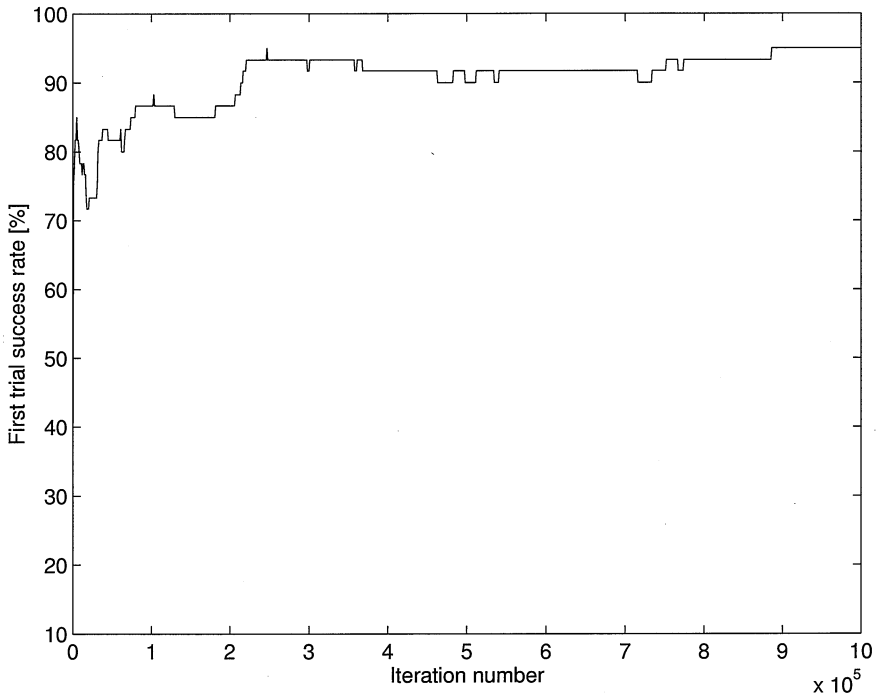

Fig. 16. First trial success rate of the current predictor trained with only the on-line samples.

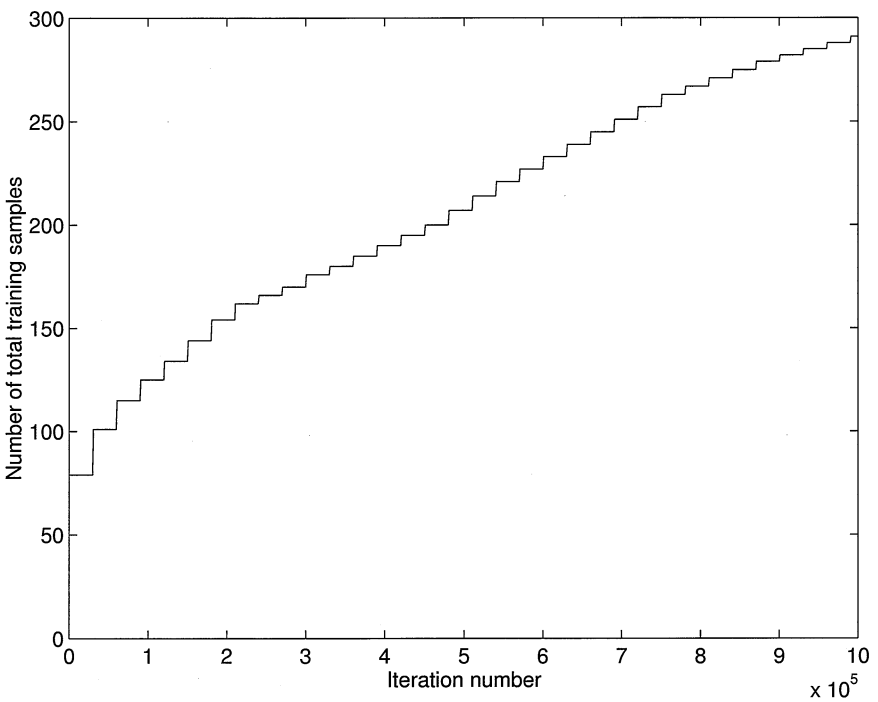

Fig. 17. Total number of generated on-line samples.

the current-prediction model. The adaptive current predictor is then developed by estimating the unknown parameters and functions in the current-prediction model. The gradient descent algorithm has been used to estimate the parameters, and an adaptive fuzzy-control technique has been used to estimate the functions. When the predicted current fails, a current-tuning method has been developed to adjust the current. In addition, an

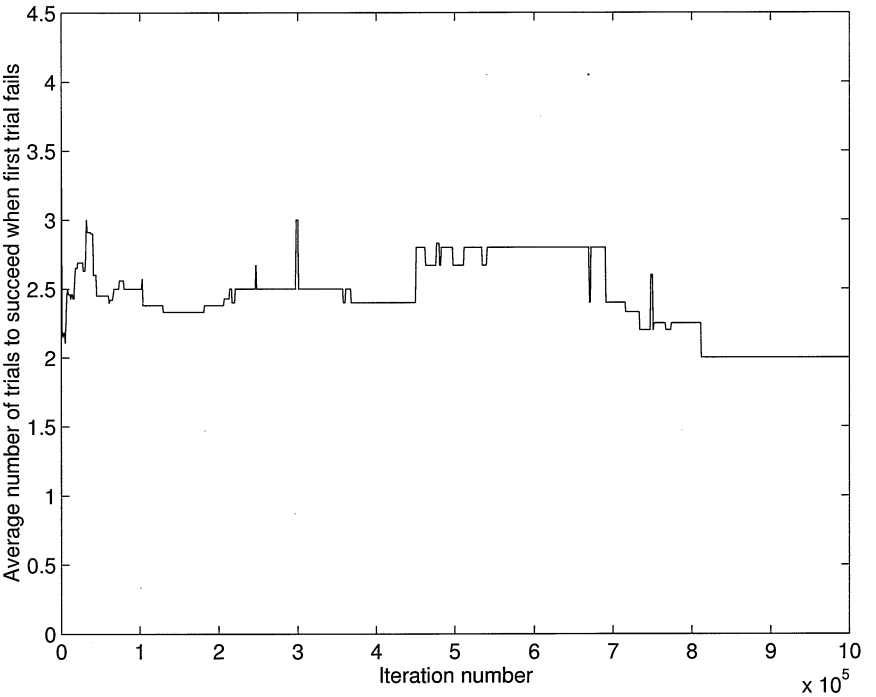

Fig. 18. Average number of trials required to complete the task when the first trial fails. (The current predictor is trained with only the on-line samples.).

on-line training-sample-generation algorithm is presented to improve the success rate of the first trial. The simulation tests with the data obtained from the storage yard have shown that the proposed controller performs well once it has been trained with the training samples collected off-line from the storage yard. It turns out to be feasible even without off-line training.

Acknowledgements

Financial support from Korea Science and Engineering Foundation through the Automation Research Center at POSTECH is gratefully acknowledged.

Appendix A

By using Eq. (2), Eq. (5) is rewritten as

$$NI = l_s f_s^{-1}\left(\frac{\phi_1}{S_{p_1}}\right) + l_m f_m^{-1}\left(\frac{\phi_{g_1}}{S_m}\right) + \frac{W_M}{W_{\phi_1}} R_0 \phi_{g_1} \qquad (A.1)$$

from which Eq. (8) follows. Similarly, Eq. (6) is rewritten as

$$l_s f_s^{-1}\left(\frac{\phi_i}{S_{p_i}}\right) = l_s f_s^{-1}\left(\frac{\phi_{i+1}}{S_{p_{i+1}}}\right) + \frac{W_M}{W_{\phi_{i+1}}} R_0 \phi_{g_{i+1}} + t_i f_s^{-1}\left(\frac{\phi_{g_{i+1}}}{S_{g_i}}\right), \quad 1 \le i \le n-1 \qquad (A.2)$$

which is equivalent to

$$\phi_i = \frac{t_i W_{\phi_i}}{t_{i+1} W_{\phi_{i+1}}} \phi_{i+1} + t_i W_{\phi_i} f_s\left(\frac{W_M R_0 \phi_{g_{i+1}}}{l_s W_{\phi_{i+1}}}\right) + t_i W_{\phi_i} f_s\left(\frac{t_i}{l_s} f_s^{-1}\left(\frac{W_M \phi_{g_{i+1}}}{S_0 W_{\phi_i}}\right)\right), \quad 1 \le i \le n-1. \qquad (A.3)$$

The first term in Eq. (A.3) corresponds to the flux caused by ϕ_{i+1} when it passes along the plate p_{i+1}, and the second and third terms are caused by $\phi_{g_{i+1}}$ when it traverses the air gap g_{i+1} and the plate p_i straight down, respectively. The third term looks rather complex but its value is relatively small because t_i for $1 \le i \le n$ ranges from 6 to 50 mm, while l_s is about 500 mm. Since t_i/l_s is small, the third term can be approximated and simplified by assuming that the function f_s is linear, i.e. the permeability of the steel is constant in p_i. Then it becomes

$$t_i W_{\phi_i} f_s\left(\frac{t_i}{l_s} f_s^{-1}\left(\frac{W_M \phi_{g_{i+1}}}{S_0 W_{\phi_i}}\right)\right) = t_i W_{\phi_i} \frac{t_i}{l_s} \frac{W_M \phi_{g_{i+1}}}{S_0 W_{\phi_i}} = \frac{W_M}{l_s S_0} t_i^2 \phi_{g_{i+1}}, \qquad (A.4)$$

and Eq. (A.3) reduces to Eq. (9).

Appendix B

From Eqs. (7), (13) and (14), and after some manipulations and rearrangements on the equations, $\partial I_n/\partial \phi_i$ for

$1 \le i \le n$ is given by

$$\frac{\partial I_n}{\partial \phi_1} = \frac{\partial \hat{F}_1}{\partial \phi_1} + \frac{\partial \hat{F}_2}{\partial \phi_{g_1}}\frac{\partial \phi_{g_1}}{\partial \phi_1} + \frac{\hat{a}}{W_{\phi_1}}\frac{\partial \phi_{g_1}}{\partial \phi_1}$$

$$= \hat{F}_1'\left(\frac{\phi_1}{t_1 W_{\phi_1}}\right)\frac{1}{t_1 W_{\phi_1}} + \hat{F}_2'(\phi_{g_1}) + \frac{\hat{a}}{W_{\phi_1}},$$

$$\frac{\partial I_n}{\partial \phi_i} = \frac{\partial I_n}{\partial \phi_{i-1}}\frac{\partial \phi_{i-1}}{\partial \phi_i} + \frac{\partial \hat{F}_2}{\partial \phi_{g_1}}\frac{\partial \phi_{g_1}}{\partial \phi_i} + \frac{\hat{a}}{W_{\phi_1}}\frac{\partial \phi_{g_1}}{\partial \phi_i}$$

$$= \frac{\partial I_n}{\partial \phi_{i-1}}\left(\frac{t_{i-1}W_{\phi_{i-1}}}{t_i W_{\phi_i}} + t_{i-1}W_{\phi_{i-1}}\hat{F}_3'\left(\frac{\phi_{g_i}}{W_{\phi_i}}\right)\right.$$

$$\left.\times\frac{1}{W_{\phi_i}} + \hat{b}\cdot t_{i-1}^2\right)$$

$$+ \hat{F}_2'(\phi_{g_1}) + \frac{\hat{a}}{W_{\phi_1}}, \quad 2 \le i \le n \tag{B.3}$$

where $\hat{F}_m'(x) = \hat{F}_m d(x)/dx$ *for* $1 \le m \le 3$ and can be computed from Eq. (20) as

$$\hat{F}_m'(x) = \frac{\sum_{r=1}^{M}\sum_{s=1}^{M}\frac{2(\bar{y}_m^s - \bar{y}_m^r)(x - \bar{x}_m^r)}{(\sigma_m^r)^2}z_m^r z_m^s}{\left\{\sum_{r=1}^{M} z_m^r\right\}^2} \tag{B.4}$$

where $z_m^r = \exp(-(x - \bar{x}_m^r/\sigma_m^r)^2)$ and $z_m^s = \exp(-((x - \bar{x}_m^s)/\sigma_m^s)^2)$ for $1 \le r \le M$.

Appendix C

From Eqs. (13), (14) and (16), $\partial E/\partial \hat{F}_1$, $\partial E/\partial \hat{F}_2$ and $\partial E/\partial \hat{F}_3$ can be computed, respectively, as

$$\frac{\partial E}{\partial \hat{F}_1} = \frac{\partial E}{\partial I_n}\frac{\partial I_n}{\partial \hat{F}_1} = -(I_n^d - I_n) \tag{C.1}$$

$$\frac{\partial E}{\partial \hat{F}_2} = \frac{\partial E}{\partial I_n}\frac{\partial I_n}{\partial \hat{F}_2} = -(I_n^d - I_n) \tag{C.2}$$

$$\frac{\partial E}{\partial \hat{F}_3} = \sum_{i=1}^{n-1}\frac{\partial E}{\partial I_n}\frac{\partial I_n}{\partial \phi_i}\frac{\partial \phi_i}{\partial \hat{F}_3} = -(I_n^d - I_n)\sum_{i=1}^{n-1}\frac{\partial I_n}{\partial \phi_i}t_i W_{\phi_i} \tag{C.3}$$

with $\partial I_n/\partial \phi_i$ for $1 \le i \le n-1$ given in Appendix B.

References

Atkinson, K.E., (1993). Elementary numerical analysis (2nd, ed.) New York: Wiley.

Fliess, M. and Lévine, J., & Rouchon, P. (1993). Generalized state variable representation for a simplified crane description. *Int. J. Control*, 58(2), 227–283.

Hayt, W.H.J. (1981). Engineering electromagnetics (4th, ed). McGraw-Hill.

Lee, J. S. and Kang, B. G., (1996), The development of magnetic sensor for plate control. Technical Report, Pohang University of Science and Technology,

Lee, J.S., & Park, B.H. (1994). The field application of study of the plate sensing and control systems, Technical Report, Research Institute of Science and Technology.

Ohnishi, E., Tsuboi, I., Egusa, T., & Uesugi, M. (1981). Automatic control of an overhead crane. *8th Triennial World Congress* (pp. 1885–1890). IFAC Control Science and Technology, Kyoto, Japan.

Scott, W.T. (1966). The physics of electricity and magnetism. (2nd, ed.) New York: Wiley.

Takagi, T., & Sugeno, M. (1985). Fuzzy identification of systems and its applications to modeling and control. *IEEE Trans. Systems. Man Cybernet., SMC*-15, 116–132,

Wang, L.X. (1994). Adaptive fuzzy systems and control: Design and stability analysis. Englewood Cliffs, NJ: Prentice-Hall.

Wang, L.X. (1997). *A course in fuzzy systems and control*. Englewood Cliffs, NJ: Prentice-Hall.

Ralph R.P. (1963). *Electricity and magnetism* (2nd ed.). Englewood Cliffs, NJ: Prentice-Hall.

Yoon, J.S., Park, B.S., Lee, J.S., & Park, H.S. (1991). Development of anti-swing control algorithm for the overhead crane. *39th Conference on Remote Systems Technology* (pp. 89–95).

Zadeh, L.A. (1965). Fuzzy sets. Inform. Control, 8, 338–353,